In-Flight Kinetic Measurements of the Aerosol Growth of Carbon Nanotubes by Electrical Mobility Classification

S. H. Kim and M. R. Zachariah*

Co-Laboratory for Nanoparticle-based Manufacturing and Metrology, Department of Chemistry and Biochemistry and Department of Mechanical Engineering, University of Maryland, College Park, Maryland 20742, and National Institute of Standards and Technology, Gaithersburg, Maryland 20899

Received: July 28, 2005; In Final Form: December 1, 2005

We describe an on-the-fly kinetic study of gas-phase growth of multiwalled carbon nanotubes. The methodology employs electrical mobility classification of the CNT, which enables a direct measure of CNT length distribution in an aerosol reactor. The specific experiment employs two mobility classification steps. In the first step we mobility classify the catalyst particle, in this case Ni, created by pulsed laser ablation, to generate a stream of monodisperse particles. This then determined the diameter of the CNT, when a hydrocarbon/H_2 mix is added in a heated aerosol reactor. A second electrical mobility classification step allows us to determine the length distribution of the CNTs. We found that CNT growth from ethylene required the addition of small amounts of water vapor, whereas growth from acetylene did not. We show that acetylene, which always has small amounts of acetone present when purchased, can provide the oxygen source to prevent catalyst coking. By varying the temperature of the growth, we were able to extract Arrhenius growth parameters. We found an activation energy for growth ∼80 kJ mol^{-1} from both acetylene and ethylene, which is considerably lower than previous works for substrate-grown CNTs (E_a = 110−150 kJ mol^{-1}). Furthermore, we observed that our aerosol CNT growth rates were about 2 orders of magnitude higher than those for substrate-grown CNTs. The dominant growth mechanism of CNT previously proposed is based upon bulk diffusion of carbon through nickel particles. However, on the basis of the lower activation energy found in this work, we proposed that the possible mechanism of gas-phase growth of CNT is correlated with both surface (E_a = 29 kJ mol^{-1}) and bulk diffusion (E_a = 145 kJ mol^{-1}) of carbon on nickel aerosol particles. Finally, the experimental approach described in this work should be amenable to other nanowire systems grown in the aerosol phase.

Introduction

Following the development of chemical vapor deposition (CVD)-assisted formation of carbon nanotubes (CNTs),[1] considerable effort has been expended in establishing the mechanisms of growth. The most favored mechanism involves the adsorption of hydrocarbon vapor on metal surfaces, leading to the catalytic formation of carbon atoms, which subsequently diffuse along the metal surface or through the metal toward the active site of CNT growth. The carbon diffusion flux through the metal is determined by the carbon concentration gradient within the metal catalyst.[2−6]

Numerous kinetic growth investigations of filamentous carbon on metal catalysts have been made to identify and validate a CNT growth mechanism.[3,5,7−9] These prior kinetic studies can be categorized into two major approaches: (i) vacuum microbalance (VMB)-based measurement of the rate of mass increase due to carbon deposition on various substrates[3,7] and (ii) electron microscopic observation of growth of carbon filaments on substrates containing catalytic metal particles.[5,8,9] Using the VMB-based approach, Bernardo and Lobo[3] and Lobo and Trimm[7] measured the rate of carbon deposition on a nickel foil with C_2H_2 as a function of temperature and obtained an activation energy of ∼130 kJ mol^{-1} for growth temperatures of 300−500 °C. At temperatures above 600 °C, a higher activation energy of ∼200 kJ mol^{-1} was observed, which was attributed to the deposition of carbon directly decomposed from gas-phase C_2H_2. Ducati et al.[8] employed a scanning electron microscope (SEM) to observe the growth rate of CNTs on polydisperse nickel particles from C_2H_2, at 550−850 °C and determined the activation energy for CNT growth to be ∼117 kJ mol^{-1}. These activation energies are comparable with the activation energy for bulk diffusion of carbon (∼145 kJ mol^{-1})[10] and are the primary supporting evidences for the carbon diffusion mechanism. In contrast there were several reports of much lower activation energy of carbon diffusion on nickel.[11,12] Using radioactive tracer techniques, Massaro and Petersen[11] performed carbon diffusion experiments on polycrystalline nickel foil between 350 and 700 °C and found the activation energy of 82 kJ mol^{-1} as an upper limit for surface diffusion of carbon.

One consideration then is to eliminate the role of the substrate in the characterization of CNT growth, by studying the growth rate on free catalytic particles. To achieve this, we have developed an aerosol production method for CNTs in a temperature-controlled environment and coupled it to an on-the-fly method for measuring CNT growth rate. The measurement employs the use of monodisperse catalyst particles from which CNTs are grown in the gas phase. The rate of growth is measured dynamically by electrical mobility classification (gas-phase electrophoresis), and from it the length of the CNTs in

* To whom correspondence should be addressed. E-mail: mrz@umd.edu.

10.1021/jp0541718 CCC: $33.50
Published on Web 02/18/2006

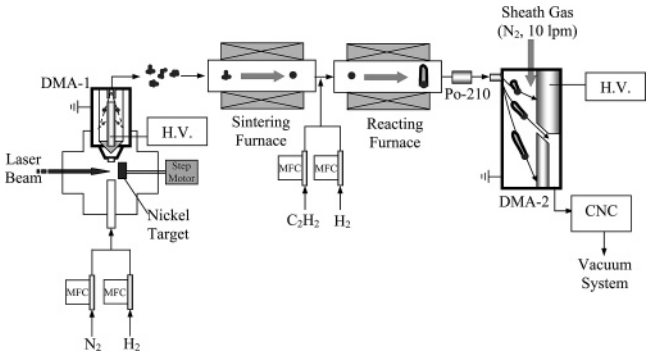

Figure 1. Schematic of laser ablation/tandem differential mobility system. DMA: differential mobility analyzer. CNC: condensation nucleus counter. MFC: mass flow controller. H.V.: high voltage power supply.

the aerosol phase. More specifically, we will describe a tandem differential mobility experiment (TDMA) method to determine the growth kinetics and activation energy of CNTs grown in the aerosol phase.

Experimental Section

The basic approach of the experiment is to size segregate growing CNTs, by mobility classification using a differential mobility classifier (DMA). Essentially, in our experiment, gas-phase electrophoresis is first used to select the diameter of the CNT to be formed, and a second electrophoretic step is employed to length select the CNT. The procedure can thus be used as either a preparatory method, or for the purposes of this work, as an on-the-fly method to determine the size distribution of CNTs grown in an arbitrary process.

The catalyst particles, in this case nickel, are generated as an aerosol and mobility classified using a DMA and then thermally annealed in the gas phase to yield spherical monodisperse particles. CNTs were then grown in-flight on the size-selected nickel aerosol particles with a thermal CVD process.[13] We employed a second DMA at the exit of thermal CVD reactor to in-situ monitor the temperature-dependent evolution of size distributions of the as-grown CNTs in the gas phase. We and others have previously employed the TDMA method to study the evolution of physical and chemical properties of particles due to condensation, evaporation, and chemical reaction.[14−18] One of the primary distinguishing features of this work from our prior work is the ability to employ the TDMA method for nanotubes.

Figure 1 shows a schematic of experimental system, which consisted of a pulsed laser ablation (PLA) particle source, and TDMA system. The PLA system consists of a 1064 nm Q-switched Nd:YAG laser beam focused with a 20 cm focal length lens to a solid nickel target. An intense laser-induced microplasma at the nickel surface, generated a vapor that was continuously swept and quenched by 1 lpm flow of nitrogen carrier gas so that nickel nanoparticles were formed by nucleation and coagulation. The addition of 50 cm^3 min^{-1} (SCCM) flow of hydrogen, along with the nitrogen carrier gas was used to suppress the possible formation of an oxide layer on the nickel particles. The nickel target was mounted on a rotating shaft with a stepper motor, so that the target could be rotated with a controlled interval to provide long-term stability in the particle generation process.

The polydisperse nickel aerosol particles generated in the PLA were then rapidly transported into a DMA which was incorporated within the ablation chamber. Because a reasonably high fraction of PLA-generated nickel particles was singly charged due to the laser-induced plasma, the DMA was operated without any auxiliary charger. The DMA was employed as a particle size selection tool and operated on the basis of gas-phase electrophoresis, by selecting particles based on equivalent electrical mobility. The details of the DMA are described elsewhere.[19,20] Briefly, the DMA typically consisted of a high voltage-connected cylindrical central rod, which was aligned coaxially with an electrical ground-connected cylindrical housing. Clean dry sheath nitrogen (∼10 lpm) was supplied around the central electrode, and the annular flow of PLA-generated aerosol particles (∼1 lpm) was introduced from the top of the DMA column. Although the majority of metal aerosols were exhausted through the bottom of DMA column, a fraction of metal aerosols with equivalent electrical mobility were classified on the balance of electrostatic attraction and drag forces and could be extracted from the instrument.

In this study, two DMAs were employed. DMA-1's function was to classify singly charged mono-area particles by their electrical mobility.[21,22] The mono-area metal nanoparticles selected from DMA-1 were subsequently sintered at the first tube furnace (hereafter referred to as the sintering furnace) at 1200 °C to form larger unagglomerated primary particles. The sintered metal nanoparticles were then introduced into the second tube furnace (hereafter referred to as the reacting furnace), where acetylene, or ethylene (∼5 SCCM) and hydrogen (∼200 SCCM) were supplied to grow carbon nanostructures on the incoming nickel aerosol nanoparticles. The sintering furnace had a 1 in. diameter × 50 cm heating length, and the reacting furnace had a 1 in. diameter × 60 cm heating length so that the residence time was ∼3 and ∼5 s at ∼1200 °C and ∼900 °C, respectively, for a fixed 1 lpm aerosol flow rate.

The aerosolized carbon nanotubes generated in the reacting furnace were then introduced into a radioactive ionizing source (Po-210) and DMA-2 for further classification based on electrical mobility. The Po-210 generated bipolar ions and produced an equilibrium charge distribution on the growing aerosol CNTs. The DMA-2 combined with a condensation nucleus counter (CNC, Model 3025A, TSI, Inc.) was used to measure the change of size distribution of the DMA-1 classified metal particles, following the gas-phase growth of CNTs.

For morphological analysis, the positively charged CNTs selected by DMA-2 were collected for ∼30 min on a TEM grid, which was placed on the electrode of an electrostatic precipitator (ESP, Model 3089, TSI, Inc.). TEM characterization was conducted with a JEOL 1210, operating at 120 kV.

Results and Discussion

Aerosol Production of Size-Controlled Nickel Particles. The nickel aerosol particles generated by the PLA were observed to be fractal-like agglomerates with ∼5 nm primary particles, as shown in Figure 2a. To extract growth kinetic parameters for nickel particle-mediated CNTs, it was necessary to make unagglomerated nickel particles with controlled and uniform diameter. To do so, we first classify the polydisperse fractal-like metal agglomerates into mono-area particles by using a DMA, in which the incoming agglomerated particles randomly rotate in the electric field, and the tumbling agglomerated particles are selected by the balance of an electrostatic attraction force and a drag force, which is proportional to its projected area diameter.[21,22] With the DMA, we sampled the Ni aerosol generated by the PLA with a fixed voltage of 1.508 kV, which enabled the selection of positively charged and mono-area agglomerated particles with a nominal electrical mobility diameter of 30 nm. These mono-area particles selected by the

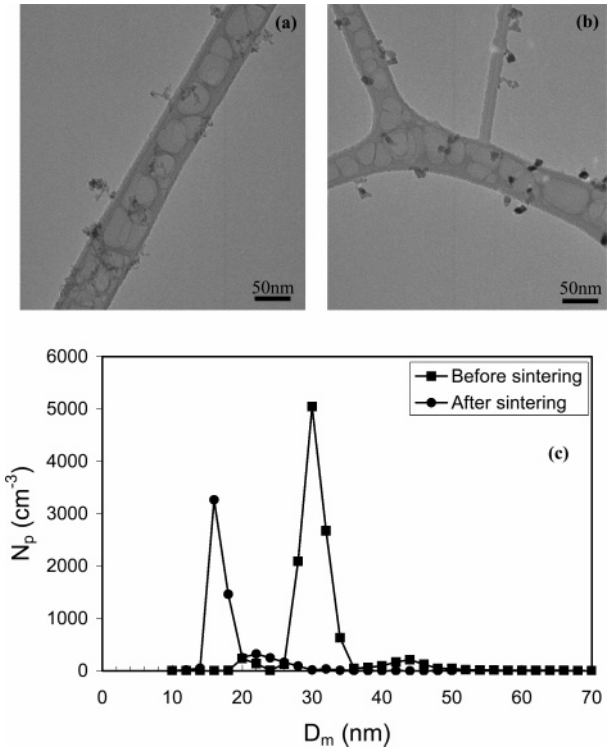

Figure 2. TEM images of 30 nm size-selected nickel particles (a) before and (b) after in-situ sintering process, and (c) TDMA size distribution measurement of the effect of sintering on 30 nm size selected particles.

DMA were subsequently made spherical in the sintering furnace at ~1200 °C, with a residence time of ~3 s. TEM analysis as shown in Figure 2b shows that the 1200 °C sintered nickel particles are indeed unagglomerated and isolated. Using the TDMA method, we have also tracked the evolution of the particle size due to temperature-dependent sintering, the results for which are detailed elsewhere.[13] An example of the result is shown in the size distributions before and after sintering using the TDMA system in Figure 2c. The initial 30 nm agglomerated nickel particles, when fully sintered and turned into isolated primary particles, are shown to have a nominal diameter of ~15 nm, with geometric standard deviation of only 1.15, indicating that the catalyst particles are indeed very monodisperse.

Morphology of Carbon Nanostructures Grown on Size-Selected Ni Aerosol Particles. The uniform Ni nanoparticles selected by DMA-1 were then mixed with C_2H_2 or C_2H_4 and H_2, and in some cases small quantities of water vapor, which reacted to grow carbon nanostructures on the nickel particles at various reacting temperatures. To identify the forms of carbon grown, samples at four different reacting temperatures were collected on TEM grids after classification in DMA-2. For these samples a fixed DMA-2 voltage was picked to pass particles that corresponded to the peak in the size distribution (i.e., the most probable growth structure). This corresponded to setting DMA-2 to pass mobility sizes (D_m) of 28 nm (400 °C), 44 nm (450 °C), 70 nm (500 °C), and 120 nm (600 °C). Figure 3 presents the TEM images of carbon nanostructures grown at the four different temperatures mentioned above. Then, using digital image software,[23] we measured the size of the resulting carbon-coated Ni particles. At a growth temperature of 400 °C, the Ni particles were found to be completely coated by a thin carbon layer (see Figure 3a). The diameter of the Ni particles was observed to be 15 ± 2 nm as expected from our sintering experiments, whereas the outer diameter of carbon-coated Ni particles was found to be 26 ± 4 nm. When the temperature was increased to 450 °C (Figure 3b), a thicker carbon layer on Ni particles was observed, and the beginnings of what look like the nucleation of fibrous carbon. Above 500 °C, as seen in Figure 3c,d, CNTs were formed, with a diameter commensurate with the uniform diameter of Ni particles passed through DMA-1. High-resolution TEM (HRTEM) analysis of carbon nanostructures grown at 600 °C (Figure 3e) indicate multiwalled nanotubes having an outer diameter of ~15 nm and composed of up to 15 walls and a hollow core.

TDMA Measurements of Aerosol CNT Growth. Recalling that our overall objective is to obtain in-flight size measurements of CNTs to extract growth rates, we begin by presenting the evolution of the CNT size distribution. For these measurements DMA-1 as before is held at a fixed voltage to select the uniform Ni particles, whereas DMA-2 combined with a condensation particle counter is scanned (see Figure 1). In a prior study we have investigated the behavior of CNTs in a mobility analyzer, the results for which we only summarize here.[24] The interpretation of the mobility distribution observed requires a consideration of how a cylindrical object might flow and orient in the electrostatic classifier. For a charged object, the separation mechanism is based on the number of charges on the object, and the charge location, and is known as electrophoresis. For an uncharged conducting object, the presence of a strong asymmetric dc electric field may induce a dipole and result in migration, also known as dielectrophoresis. As such, a dielectrophoresis separation mechanism would require that the nanotube be aligned parallel to the direction of the *E*-field as it flowed in the classifier and implying that the dielectric force can suppress random Brownian tumbling of the nanotube. In our prior study we have shown that dielectrophoretic force is quite weak for the field employed here. By evaluating the integral of the torque over some angular displacement away from the electric field parallel, we can evaluate if the ambient thermal energy is sufficient to disorient the CNT. We find for a singly charged nanotube with a diameter of 15 nm, and any length shorter than 1000 nm, that the Brownian thermal energy is sufficient to result in free rotational motion for fields up to ~3 kV/cm.[24,25] A freely tumbling nanotube will present a drag force proportional to its projected surface area. And, for diameter-selected nanotubes, this implies that the electrophoretic separation is directly proportional to the nanotube length. However, as the electric field strength in a DMA is increased, longer nanotubes (>1000 nm) tend to be aligned by the strong electric field applied (>~3 kV), which resulted in a reduction in the drag force so that the DMA-selected length of the CNTs was observed to be longer than expected. This might lead to an increase in the deviation between the length determined by TEM and DMA.

We begin our studies by characterizing the role of hydrogen on the growth of carbon nanostructures. Figure 4 presents the evolution of the size distribution of size-selected Ni particles reacting with three different C_2H_2/H_2 mixtures at various temperatures. In the absence of H_2 (Figure 4a), the growth of carbon nanostructures on initially uniform Ni particles ceased at a mean size of ~28 nm regardless of the temperature, up to ~600 °C. This behavior is well-known and resulted from the coking of the catalyst particle.[26] In the absence of hydrogen, which serves as an etching agent, the Ni particles are rapidly deactivated due to the carbon deposition, which blocks any further catalytic reaction with gas-phase species. However, addition of hydrogen, as expected, promotes growth, as seen in Figure 4b,c. For a hydrogen flow rate of ~50 SCCM, which

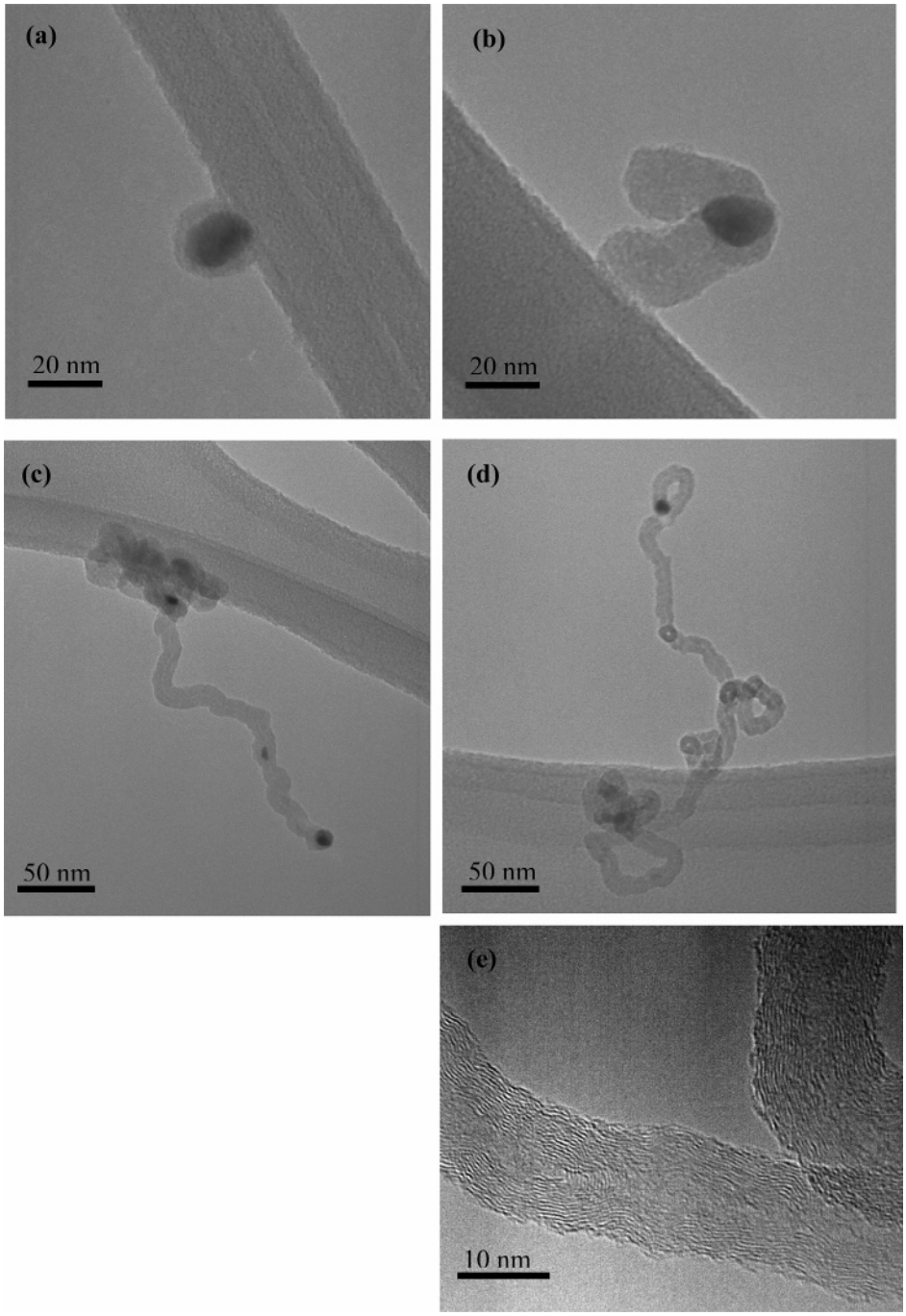

Figure 3. TEM images of gas-phase-grown carbon nanostructures collected at different temperatures (equivalent mobility size): (a) 400 °C (D_m = 28 nm); (b) 450 °C (D_m = 44 nm); (c) 500 °C (D_m = 70 nm); (d) 600 °C (D_m = 120 nm); (e) 600 °C (D_m = 120 nm) [HRTEM]. [Experimental conditions: 5 SCCM C_2H_2, 50 SCCM H_2].

corresponds to a H_2/C_2H_2 of 10 (see Figure 4b), we observe a steady increase in the size distribution with increasing temperature up to a temperature of ~600 °C, and this is presumably amorphous carbon particles formed from thermal cracking of C_2H_2 at high temperatures. Above ~600 °C, growth ceases; however, increasing the hydrogen concentration by a factor of 2 resumes the growth, as seen in Figure 4c, which implies that the presence of a sufficient amount of hydrogen can maintain the activity of catalysts by gasifying (or etching) the carbon deposited on the catalyst surface. A further increase of H_2 (>200 SCCM, H_2/C_2H_2 of 40) did not appreciably change the CNT growth dynamics.

Looking at particle size distributions shown in Figure 4c, we see no appreciable change in mean size below 300 °C (D_m ~ 15 nm), and the size distribution observed is just that of the unreacted nickel, and indicates little or no catalytic decomposition of acetylene at these low temperatures. Beginning at ~400 °C, we see a size increase in the particle size distribution (PSD) and the disappearance of the D_m ~ 15 nm peak, indicating that the growth of carbon structures is occurring on the Ni particles. This latter point was confirmed by the addition of C_2H_2 and H_2 without catalyst particles and resulted in no particulates detected with the CNC, between 400 and 700 °C. However, above ~800 °C, the formation of amorphous carbon particles was observed in the absence of the catalytic particles and appeared as < 20 nm particles at very high number concentrations. This is consistent with the electron microscopy observation of Johnson and Anderson,[27] who reported the formation of carbon particles

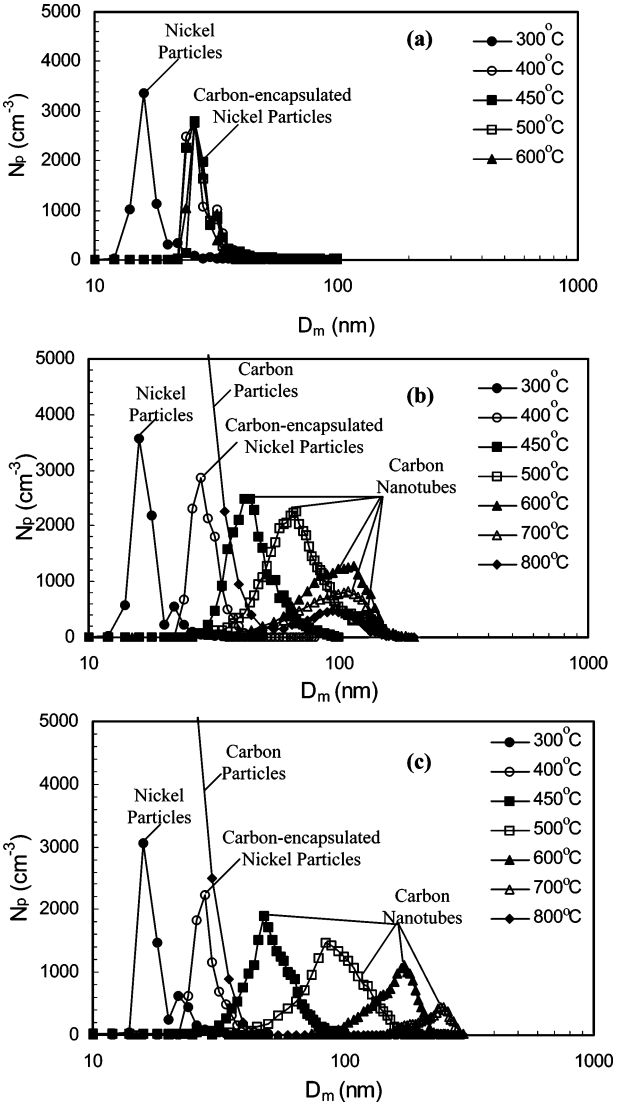

Figure 4. Temperature-dependent evolution of TDMA size distribution of carbon nanostructures grown on 15 nm Ni particles reacting with 5 SCCM C_2H_2 and (a) 0 SCCM H_2, (b) 50 SCCM H_2, and (c) 100 SCCM H_2.

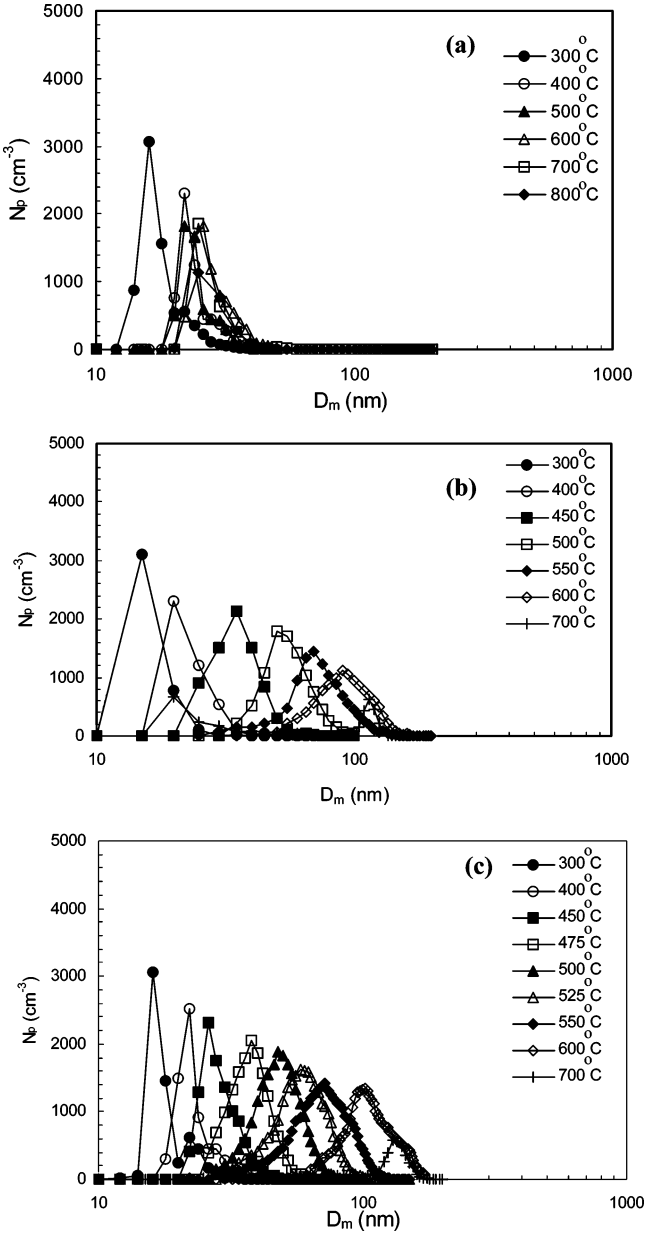

Figure 5. Temperature-dependent evolution of TDMA size distribution of carbon nanostructures grown on 15 nm Ni particles reacting with 5 SCCM C_2H_4 and 100 SCCM H_2 in the presence of (a) no oxidizer, (b) 150 ppm C_3H_6O, and (c) 200 ppm H_2O.

in the pyrolysis of C_2H_2 at temperatures between 700 and 900 °C in the absence of catalytic particles. In the presence of nickel particles, and at the highest hydrogen concentration used in our experiments, we always observed a steady increase in size distribution for fixed residence time as the temperature was increased.

Similar experiments were also conducted with ethylene (C_2H_4) as another hydrocarbon source. Figure 5a presents TDMA results and shows that, using a 15 nm Ni catalyst, the resulting size distribution had an arrested growth at about $D_m \sim 30$ nm regardless of temperature. The morphology of these particles, regardless of temperature, is similar to that shown in Figure 3a and indicates that the catalyst was coked and formed carbon-encapsulated Ni particles. Indeed, further increasing the hydrogen concentration did not make any significant difference. This result is also consistent with the report by Bernardo and Lobo[3] that carbon deposition from C_2H_2 is much faster than from 1-butene. Though no explanation was given, we note that C_2H_2 has a positive heat of formation (rare for a hydrocarbon), implying that it is thermodynamically unstable relative to solid carbon. As such, it can be decomposed explosively at high pressures. As a result, acetylene, when purchased in a gas cylinder, actually has some acetone (C_3H_6O) added as a radical scavenger, to prevent explosion. It is possible, then, that the presence of oxygen in the form of C_3H_6O in C_2H_2 could also promote the formation of CNTs on Ni particles by selectively removing amorphous carbon.

According to both Hata et al.[28] and Cao et al.,[29] water vapor is employed as a mild oxidizer as compared with oxygen or carbon monoxide. They found the etching effect of water on amorphous carbon. TGA and TEM analysis confirmed that (i) a controlled amount of water vapor addition does not oxidize the surface of carbon nanotubes at growth temperatures of 200−1000 °C and (ii) amorphous carbon grown on both the CNT surface and a metal surface was removed by a water-induced oxidation environment. However, large amounts of water caused the formation of defects on the CNT surface. On the basis of these works, we also employed water vapor as a mild oxidizer.

To assess the effect of oxygenate addition on the growth of carbon nanostructures, we added a controlled amount of acetone

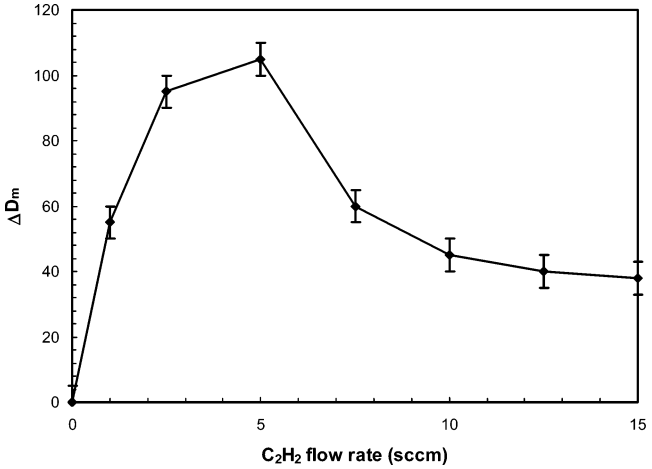

Figure 6. Mobility size change of carbon nanostructures as a function of the amount of C_2H_2 addition on nickel particles selected by DMA-1.

(~150 ppm) or water (~200 ppm) as a weak oxidizer during growth from ethylene. The effects of acetone and water addition are presented in Figure 5b,c and clearly show, particularly in comparison to Figure 5a, that the addition of acetone and water can significantly change the growth dynamics. In this case growth from ethylene is quite rapid and indicates clearly that catalyst coking can be prevented with oxygenates. We also observed that further increases in water did not change the resulting TDMA size distribution, indicating that etching with water is relatively fast and, beyond the threshold concentration needed, has no effect. However, unlike water addition, increasing acetone concentration (>~200 ppm) was found to act as a carbon source and enable the growth of carbon nanotubes even in the absence of ethylene. As such, we maintained the acetone concentration ~150 ppm. By comparison, we observed that water-assisted promotion of CNT growth did not occur for C_2H_2 and is consistent with the hypothesis that growth from acetylene is already mediated with an etchant (i.e., acetone), whereas other hydrocarbons require addition of an oxygen containing species to prevent coking of the catalyst.

To probe dependence of the nanotube growth rate on the hydrocarbon concentration, we performed a series of measurements as a function of hydrocarbon addition. On the basis of the total number concentration (~10^5 cm^{-3}) of Ni nanoparticles selected by DMA-1, the size change of carbon nanostructures was found to increase with increasing amount of C_2H_2 up to ~5 sccm, as seen in Figure 6. However, beyond that concentration, growth dropped off, presumably as a result of catalyst coking. This also means that the relation between hydrocarbon pressure and growth rate of carbon nanostructures is nonmonotonic and therefore not easily amenable to description in a rate law containing partial pressure of hydrocarbon. As such, the kinetic parameters extracted later in this paper were limited to the optimum nanotube's growth conditions for the case of 5 sccm C_2H_2 addition.

Extracting Kinetic Parameters for the Gas-Phase Growth of CNTs. Next we turn our attention to extracting kinetic rate parameters from the TDMA measurements. To obtain kinetic parameters, we will fit our data to an Arrhenius form for the rate of size increase (dD_m/dt) in a manner analogous to studies we have conducted on soot oxidation.[16−18]

$$\dot{D}_m = A \exp\left[-\frac{E_a}{RT}\right] \tag{1}$$

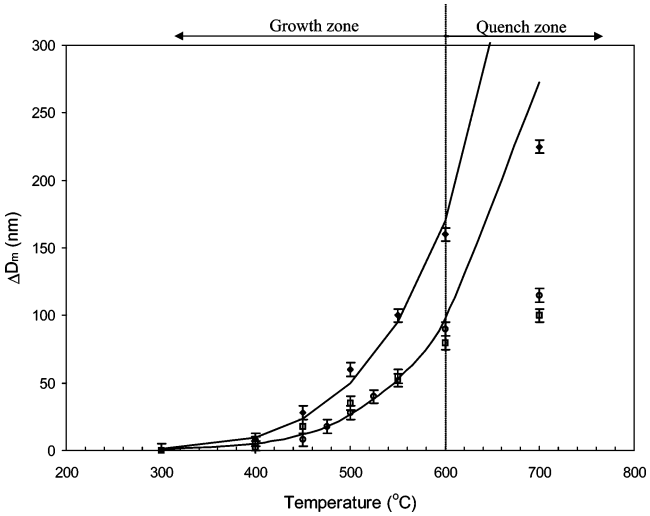

Figure 7. Comparison of the size change of carbon nanostructures as a function of temperature for 15 nm initial size of Ni particles. Solid lines are fits based upon the kinetic parameters of Arrhenius equation. Solid circles are for the case of Ni reacted with C_2H_2 ($E_a = 77 \pm 2$ kJ mol^{-1}, $A = 1.4 \times 10^6$ nm s^{-1}). Open squares are for the case of Ni reacted with C_2H_4 with C_3H_6O addition, and open circles are for the case of Ni reacted with C_2H_4 with H_2O addition ($E_a = 80 \pm 2$ kJ mol^{-1}, $A = 1.4 \times 10^6$ nm s^{-1}).

where A is the preexponential factor, T is the temperature, E_a is the activation energy for CNT growth, and R is the gas constant.

To relate the size change measured by the TDMA experiment with the Arrhenius equation, eq 1 was integrated over the length of heating zone in the reacting furnace as follows,

$$\Delta D_m = \int_0^x \frac{\dot{D}_m(x)}{u(x)}\,dx \tag{2}$$

where x is a horizontal position in the tube, X is the length of the tube, and u is the flow velocity, which is calculated as

$$u(x) = \frac{4}{3}u_m\frac{T(x)}{T_o} \tag{3}$$

where $^4/_3 u_m$ is the peak flow velocity of carrier gas calculated from volume flow rate and the cross sectional area of the flow tube under the assumption of laminar flow.

Figure 7 presents the size increase measured by the TDMA system (symbols) as a function of temperature. The solid lines represent a best fit of the data to the Arrhenius expression (eq 2) integrated over the length of the reactor. The fit yields an activation energy of 77 ± 2 kJ mol^{-1} and preexponential factor of 1.4×10^6 nm s^{-1} for acetylene, and a marginally higher ~80 ± 2 kJ mol^{-1} activation energy for ethylene. Our measured activation energy falls between that reported for surface (29 kJ mol^{-1} [30]) and bulk (145 kJ mol^{-1} [10]) diffusion of carbon in nickel.

On the basis of the activation energy, we may consider a possible mechanism for the rate controlling process for CNT growth. The catalytic formation of carbon began at ~400 °C, where Ni particles were found to be fully encapsulated by carbon. At ~400 °C, carbon diffusion through Ni particles ($D = 9.01 \times 10^{-12}$ cm^2 s^{-1} [11]) would be very slow due to low solubility of carbon in Ni ($S = 7.54 \times 10^{-4}$ g cm^{-3} [31]). The growth rate of carbon in Ni particles having ~15 nm in diameter at 400 °C is calculated to be ~0.2 nm s^{-1}. At low temperatures (~400 °C), the growth of carbon should be only weakly dependent on the bulk diffusion of carbon and is presumably

dominated by the surface diffusion, leading to the growth of carbon locally on the Ni particle. At higher temperatures, ~700 °C, the growth rate of CNTs is ~200 nm s^{-1} with $D = 1.94 \times 10^{-9}$ cm^2 s^{-1} and $S = 7.05 \times 10^{-3}$ g cm^{-3}. The D and S are diffusivity and solubility data measured by Lander et al.[31]

At intermediate temperatures, 400−700 °C, the amount of carbon dissolved in Ni increases exponentially,[31] while simultaneously bulk diffusion within carbon is also much faster, so that the graphitic basal plane on the Ni particle surface is continuous and results in nanotube formation. The excess carbon on the surface of Ni particles would also diffuse along the surface to incorporate under the graphitic plane, promoting nanotube growth.[32] However, at much higher temperatures of 700−900 °C, the rapid increase of amorphous carbon directly formed from thermal cracking of the hydrocarbon feedstock should lead to coking and the retardation of CNT growth. This latter effect can be observed in Figure 7 where at higher temperatures the Arrhenious fit breaks down and we refer to this regime in the figure as a "quench zone".

Comparison of the Gas-Phase Growth Rate of CNTs with Substrate-Grown Growth Rates. To estimate the growth rate of CNTs directly from the TDMA measurement, we extracted the length distribution from the mobility size distributions as we have described elsewhere.[24] Briefly, the as-grown uniform CNTs introduced into the second DMA are freely tumbling in a relatively low electric field (<~3 kV/cm), and the mobility diameter (D_m) of CNTs selected was found to be linearly proportional to the projected area diameter (D_A), which was obtained from the combination of TEM images and digital image software analysis.[23] This means that diameter-selected CNTs with equivalent mobility size are of uniform length when selected by the second DMA. With the relation between D_m and D_A ($D_A = C_1 D_m + C_2$, where $C_1 = 1.1621$, $C_2 = -8.9131$,[23]), we calculated the length of CNTs with the following equation,

$$L_f = \frac{\pi D_A^{\,2}}{4D_f} = \frac{\pi}{4D_f}(C_1 D_m + C_2)^2 \qquad (4)$$

where L_f is the length of the CNT, D_f is the diameter of the CNT, and D_A is the projected area diameter of the CNT. The constants C_1 and C_2 provide the relationship between mobility diameter and projected area diameter and were obtained in a prior study where mobility classified fibers were deposited on TEM grids and digitized to obtain the projected area diameter.[22,24] We can use the number mean mobility diameters from the CNT mobility size distributions (see Figure 4c) and convert them into an average length of the nanotubes using eq 4. The growth rate is then calculated by dividing the average length of nanotubes by the residence time in the flow tube.

Figure 8 presents an Arrhenius plot for the growth rate of CNTs and selected previous studies. Despite the fact that there are various studies of gas-phase growth of CNTs,[33−35] none of these studies have determined the length distribution or the growth rate in a manner suitable for comparison. Rather, we have chosen what we believe to be careful studies of growth rates on surfaces. In those studies, CNTs were grown from the catalyzed decomposition of acetylene at ~600 °C on SiO_2 films containing polydisperse Ni islands of 15−40 nm in diameter.[5,8] Baker et al.[5] employed C_2H_2 (~2 Torr) and H_2 (~1 Torr) to grow CNTs, and Ducati et al.[8] employed C_2H_2 (~75 sccm) and NH_3 (~200 sccm) at a total pressure of 4 Torr. For direct comparison of our CNT aerosol growth rate, with that of substrate-grown CNTs, we normalized the growth rate with the amount of acetylene addition for each experimental condition.

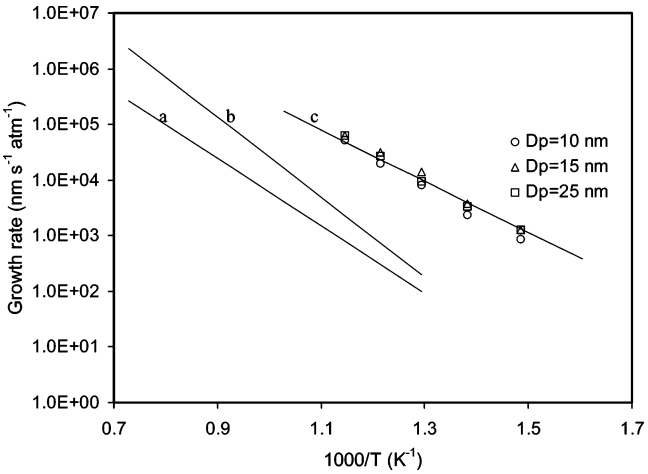

Figure 8. Growth rate comparison of this work, with selected prior studies (substrate-grown) as a function of temperature: (a) Ducati et al.,[8] $E_a = 117$ kJ mol^{-1}; (b) Baker et al.,[5] $E_a = 138$ kJ mol^{-1}; (c) current approach, $E_a = 77 \pm 2$ kJ mol^{-1}).

These results are also plotted as the solid lines in Figure 8 and indicate growth rates that are ~100 times smaller than those for our aerosol-grown CNTs. The reasons for this difference are still not clear; however, we would certainly expect that for base-growth material, the mass transfer rate would be significantly slower than that for the aerosol process. The other issue may also have to do with chemical interference from the substrate, itself. Baker and Chludzinski[5] showed, for example, that the addition of various additives (Mo, Si, and W) on the catalyst−substrate resulted in the significant decrease in the rate of carbon filament growth. The speculation is that additives were incorporated into the catalysts, resulting in a decrease in carbon solubility. Another possible reason for higher growth rate of CNTs in the gas phase may be related to the effect of primary particle size on the growth rate of CNTs. To assess this possibility, we test the growth of CNTs on using Ni aerosol of 10, 15, and 25 nm diameter. These results are also presented in Figure 8 (symbols) and indicate no significant size dependent growth. This suggests that the dominant factor for determining the growth rate of CNTs in the gas phase is not the primary catalysts size, but the growth temperature for promoting the catalytically formed carbon, diffusion and solubility, and the presence of hydrogen and/or weak oxidizer for preventing the deactivation of catalyst aerosol surface for the deposition of amorphous carbon.

Given that our growth is conducted in the absence of a substrate, and that mass-transfer effects from the gas phase would not be rate limiting, one might reasonably argue that the observation of the growth rates on substrate-grown materials are constrained by vapor-phase mass-transfer effects and that, along with possible poisoning of the catalyst from the substrate,[5] these are the most likely explanations as to why our growth rates are so much higher.

Conclusions

In this paper, we have investigated the kinetics of gas-phase growth of CNTs using on-the-fly mobility characterization of the length of CNTs, using a TDMA approach. On the basis of an activation energy of ~80 kJ mol^{-1} found for size-selected Ni aerosol particles reacting with acetylene or ethylene, we proposed that the gas-phase growth of CNTs is promoted by both surface diffusion ($E_a = 29$ kJ mol^{-1}) of carbon on nickel particles and bulk diffusion ($E_a = 145$ kJ mol^{-1}) of carbon

through nickel in the temperature range 400−600 °C. At higher temperatures (>600 °C), the growth of CNTs is significantly quenched by partial encapsulation of the catalyst particles due to the direct deposition of amorphous carbon. Addition of an oxygen containing species in low concentration was found to be a necessary condition to prevent catalyst coking. We found that growth rates for aerosol-grown CNT were as much as 2 orders of magnitude higher than the corresponding growth rates of substrate-grown CNTs.

Acknowledgment. We gratefully acknowledge HRTEM analysis performed by Dr. Chongmin Wang and Dr. Mark Engelhard in the Environmental Molecular Sciences Laboratory, a national scientific user facility sponsored by the Department of Energy's Office of Biological and Environmental Research and located at Pacific Northwest National Laboratory.

References and Notes

(1) Ren, Z. F.; Huang *Science* **1998**, *282*, 1105.
(2) Baker, R. T. K.; Barber, M. A.; Harris, P. S.; Feates, F. S.; Waite, R. J. *J. Catal.* **1972**, *26*, 51.
(3) Bernardo, C. A.; Lobo, L. S. *J. Catal.* **1975**, *37*, 267.
(4) Rostrup-Nielsen, J. *J. Catal.* **1977**, *48*, 155.
(5) Baker, R. T. K.; Chludzinski, J. J., Jr. *J. Catal.* **1980**, *64*, 464.
(6) Kock, A. J. H. M.; De Bokx, P. K.; Boellaard, E.; Klop, W.; Geus, J. W. *J. Catal.* **1985**, *96*, 468.
(7) Lobo, L. S.; Trimm, D. L. *Nature* **1971**, *234*, 15.
(8) Ducati, C.; Alexandrou, I.; Chhowalla, M.; Amaratunga, G. A. J.; Robertson, J. *J. Appl. Phys.* **2002**, *92*, 3299.
(9) Lee, Y. T.; Kim, N. S.; Park, J.; Han, J. B.; Choi, Y. S.; Ryu, H.; Lee, H. J. *Chem. Phys. Lett.* **2003**, *372*, 853.
(10) Diamond, S.; Wert, C. *Trans. AIME* **1967**, *239*, 705.
(11) Massaro, T. A.; Petersen, E. E. *J. Appl. Phys.* **1971**, *42* (13), 5534.
(12) Cooper, B. J.; Trimm, D. L.; Wilkinson, A. *London Int. Carbon-Graphite Conf., 4th* **1974** (prepr).
(13) Kim, S. H.; Zachariah, M. R. *J. Nanoparticle Res.*, submitted.
(14) Liu, B. Y. H.; Pui, D. Y. H.; Whitby, K. T.; Kittelson, D. B.; Kousaka, Y.; McKenzie, R. L. *Atmos. Environ.* **1978**, *12* (1−3), 99.
(15) McMurry, P. H.; Takano, H.; Anderson, G. R. Study of the ammonia (gas)-sulfuric acid (aerosol) reaction rate. *Environ. Sci. Technol.* **1983**, *17*, 347.
(16) Higgins, K. J.; Jung, H.; Kittelson, D. B.; Roberts, J. T.; Zachariah, M. R. *J. Phys. Chem. A* **2002**, *106*, 96.
(17) Higgins, K. J.; Jung, H.; Kittelson, D. B.; Roberts, J. T.; Zachariah, M. R. *Environ. Sci. Technol.* **2003**, *37*, 1949.
(18) Kim, S. H.; Fletcher, R. A.; Zachariah, M. R. *Environ. Sci. Technol.* **2005**, *39*, 4021.
(19) Knutson, E. O.; Whitby, K. T. *J. Aerosol Sci.* **1975**, *6*, 443.
(20) Kim, S. H.; Woo, K. S.; Liu, B. Y. H.; Zachariah, M. R. *J. Colloid Interface Sci.* **2005**, *282* (1), 46.
(21) Rogak, S. N.; Flagan, R. C.; Nguyen, H. V. *Aerosol Sci. Technol.* **1993**, *18*, 25.
(22) Jung, H.; Kittelson, D. B.; Zachariah, M. R. *Combust. Flame* **2003**, *135*, 227.
(23) Image J, National Institutes of Health, http://rsb.info.nih.gov/nih-image.
(24) Kim, S. H.; Zachariah, M. R. *Nanotechnology* **2005**, *16*, 2149.
(25) Lilienfeld, P. *J. Aerosol Sci.* **1985**, *16* (4), 315.
(26) La Cava, A. I.; Bernardo, C. A.; Trimm, D. L. *Carbon* **1982**, *20* (3), 219.
(27) Johnson, G. L.; Anderson, R. C. *Proc. Conf. Carbon, 5th* **1962**, *1*, 395.
(28) Hata, K.; Futaba, D. N.; Mizuno, K.; Namai, T.; Yumura, M.; Iijima, S. *Science* **2004**, *306*, 1362.
(29) Cao et al. *J. Mater. Res.* **2001**, *16* (11), 3107.
(30) Mojica, J. F.; Levenson, L. L. *Surf. Sci.* **1976**, *59*, 447.
(31) Lander, J. J.; Kern, H. E.; Beach, A. L. *J. Appl. Phys.* **1952**, *23* (12), 1305.
(32) Helveg, S.; Lopez-Cartes, C.; Sehested, J.; Hansen, P. L.; Clausen, B. S.; Rostrup-Nielsen, J. R.; Abild-Pedersen, F.; Norskov, J. K. *Nature* **2004**, *427*, 426.
(33) Ci, L.; Li, Y.; Wei, B.; Liang, J.; Xu, C.; Wu, D. *Carbon* **2000**, *38*, 1933.
(34) Ago, H.; Ohshima, S.; Uchida, K.; Yumura, M. *J. Phys. Chem. B* **2001**, *105* (43), 10453.
(35) Nasibulin, A. G.; Moisala, A.; Brown, D. P.; Jiang, H.; Kauppinen, E. I. *Chem. Phys. Lett.* **2005**, *402*, 227.